

RSC Advances



This is an *Accepted Manuscript*, which has been through the Royal Society of Chemistry peer review process and has been accepted for publication.

Accepted Manuscripts are published online shortly after acceptance, before technical editing, formatting and proof reading. Using this free service, authors can make their results available to the community, in citable form, before we publish the edited article. This *Accepted Manuscript* will be replaced by the edited, formatted and paginated article as soon as this is available.

You can find more information about *Accepted Manuscripts* in the [Information for Authors](#).

Please note that technical editing may introduce minor changes to the text and/or graphics, which may alter content. The journal's standard [Terms & Conditions](#) and the [Ethical guidelines](#) still apply. In no event shall the Royal Society of Chemistry be held responsible for any errors or omissions in this *Accepted Manuscript* or any consequences arising from the use of any information it contains.

Deposition of Pd-Fe nanoparticles onto carbon spheres with controllable diameters and applied for CO catalytic oxidation

Weiliang Han, Zhicheng Tang*, Peng Zhang, Gongxuan Lu

(State Key Laboratory for Oxo Synthesis and Selective Oxidation, and National Engineering Research Center for Fine Petrochemical Intermediates, Lanzhou Institute of Chemical Physics, Chinese Academy of Sciences, Lanzhou, 730000, China)

*Corresponding author. Tel.: +86-931-4968083, Fax: +86-931-8277088, E-mail address: tangzhicheng@licp.cas.cn (Z.Tang).

Abstract

In this paper, a series of Pd-Fe/carbon spheres (CSs) catalysts were prepared by a co-precipitation method and applied in the low temperature CO oxidation reaction. The effect of particle size of carbon spheres, calcination temperature of catalysts, Pd loadings and H₂ reduction were investigated in detail. SEM and TEM characterization of carbon spheres which were prepared by hydrothermal method indicated non-porous structure, and the CSs surface was covered by Pd-Fe composites after the catalysts preparation. The XPS characterization of catalysts showed that there were rich active oxygen species, more FeO(OH) species and more tetravalent Pd (PdO₂) species on the surface of Pd-Fe/CSs catalyst. These factors would be helpful for CO oxidation. When Pd loading was 1.0wt.%, the Pd-Fe/CSs (CSs were prepared by 1.0 molL⁻¹ glucose solutions) catalyst which was calcined at 200 °C without H₂ reduction had the highest activity.

Keywords: Carbon spheres; Hydrothermal method; CO oxidation; Noble metal catalyst

1 Introduction

Catalytic oxidation of CO is of great importance because of its wide applications in such as air purification, CO gas sensors and vehicle exhaust pollution control [1-3], etc. Among all catalysts for CO catalytic oxidation, Pd catalysts have attracted considerable attention because of its stability. However, the activity of Pd catalysts is lower than that of Au and Pt catalysts in CO oxidation [4-6]. So, recent studies are focused on the activity rise of Pd catalyst. Satauma [5] et al also investigated the effect of supports (CeO_2 , TiO_2 , Al_2O_3 , ZrO_2 , and SiO_2) on CO oxidation over Pd catalysts, which indicated that oxygen storage property of metal oxide support was one of the activity-controlling factors for CO oxidation. We had prepared a series of Pd-Ce supported ZSM-5 zeolite catalysts by co-impregnation method, and found that the properties of ZSM-5 zeolite had a strong influence for CO oxidation in the previous work [7]. From these literatures, it is seen that the support has important influence on the catalytic performance for low temperature CO catalytic oxidation.

Carbon spheres (CSs) are widely used in adsorption, catalysis and catalyst supports, etc, due to their advantages of minimal surface energies and controllable sizes, morphologies, chemical properties and high mechanical stability [8-10]. Various approaches have been used to prepare CSs, such as chemical vapor deposition [11, 12], high-temperature pyrolysis [13], etc. Yet these methods require sophisticated equipments, rigorous conditions or catalysts. Therefore it is of great significance to

explore energy-saving and cost-effective routes to fabricate CSs.

The hydrothermal method is unique because of its simple operational and mild reaction condition requirements. Since first studies, the interest on the hydrothermal treatment for the preparation of CSs has increased along the years [14-16]. Wang et al. [14] reported carbon microspheres with diameters of several micrometers had been synthesized by hydrothermal treatment of methylcellulose sol at 400 °C, and discussed the formation mechanism of these spheres based on the feature of the reaction system. Liu et al. [15] prepared CSs with controllable sizes and rich in oxygen-containing groups using a simple hydrothermal treatment of glucose, the effects of the hydrothermal parameters, including the concentration of glucose, reaction temperature, duration, and the second hydrothermal treatment were investigated. Wang et al [16] fabricated CSs with amino groups on their surface successfully by hydrothermal approach with ammonia in the precursor solution.

Pd-Fe-based catalyst displays excellent activity on CO oxidation [17-19]. Machida et al. [17] reported bimetal nanoparticles of Pd-Fe were deposited onto CeO₂ by using dual arc-plasma to study their structures and catalytic properties for CO oxidation, the result showed the bimetal nanoparticle catalysts exhibited a higher catalytic activity for CO oxidation, and the activity was further enhanced even after thermal ageing at 900 °C in H₂O/air. Lu et al. [18] prepared Pd-Fe-O_x catalysts supported on SBA-15, CeO₂ nano-particles with rich (111) facets and CeO₂ nano-rod with rich (200) facets, the results showed that when CeO₂ nano-rod was used as a support, Pd-Fe-O_x catalyst exhibits higher activity ($T_{100} = 10$ °C), resulting from the

rich (200) facets of CeO₂ nano-rod which leads to a formation of large numbers of the oxygen vacancies on the surface of Pd-Fe-Ox catalysts. Deng et al. [19] found that Pd catalysts supported on ferric-hydroxide were prepared by a co-precipitation method without calcinations exhibited high activity for CO oxidation.

These results suggested that Pd-Fe-based catalysts showed superior activity for CO oxidation. But Pd-Fe-based catalysts is powder according to the above literatures, it is difficult to apply in practice. How to load Pd-Fe onto structure support is important for promoting the application of Pd-Fe-based catalyst. Carbon sphere own abundant surface oxygen species, controllable sizes, regular shape, ect. Synthesizing process of carbon spheres is simple and costs less. It may be a superior support of catalyst. Thus, it is significant to the application of the Pd-Fe-based catalyst that Pd-Fe nanoparticles are deposited onto carbon spheres.

In this paper, CSs with controllable sizes was used as support and a series of Pd-Fe/CSs catalysts were prepared successfully by co-precipitation (CP) method and applied to low temperature CO oxidation. The catalysts were characterized by XRD, XPS, BET, FE-SEM and HR-TEM in detail.

2 Experimental

2.1 Synthesis of CSs

A glucose solution (0.1-1.5molL⁻¹, 80 mL) was transferred into a stainless-steel autoclave with a 60mL capacity, and was autoclaved at 180 °C for 7 h. Then, the solution was cooled to room temperature. The black precipitate was collected and sequentially washed with water, anhydrous ethanol. Then the precipitate was dried at

80 °C for 6 h. The obtained brown solid was identified as CSs.

2.2 Preparation of Catalyst

The Pd-Fe/CSs catalyst was prepared by co-precipitation method. 0.5g CSs were firstly suspended in Na₂CO₃ solution. Taken Pd(NO₃)₂ solution and Fe(NO₃)₃ solution were added to a separating funnel. When plug was opened, the mixture solutions of Pd(NO₃)₂ and Fe(NO₃)₃ flowed to Na₂CO₃ solution contained CSs support. Then Na₂CO₃ solution was added to adjust pH and aged for 3h. At last, the solution was filtered and washed with distillation water. The resulting solid was dried at 60 °C for overnight and subsequently calcined at 200 °C for 4 h. The Pd Loading amount was adjusted from 0.3% to 1.0%. Fe loading amount was 50 wt.%.

Pd-FeOx was prepared according to above method without CSs.

2.3 Catalyst Characterization

Powder X-ray diffraction (XRD) analysis was performed to verify the crystallographic phases present in carbon spheres. XRD patterns of the samples were recorded on a Rigaku D/MAX-RB X-ray diffractometer with a target of Cu K α operated at 60 kV and 55 mA with a scanning speed of 0.5°min⁻¹ and a scanning angle (2 θ) range of 10-80°.

Chemical states of the atoms in the catalyst surface were investigated by X-ray photoelectron spectroscopy (XPS) on a VG ESCALAB 210 Electron Spectrometer (Mg K α radiation; $h\nu = 1253.6$ eV). XPS data were calibrated using the binding energy of C1s (284.6 eV) as the standard.

The surface morphologies of the carbon spheres were also determined by using

field emission scanning electron microscopy (FE-SEM) in combination with Energy Dispersive X-ray analysis on an ESEM-FEG/EDAX Philips JSM-6701F instrument operating at 20 kV using catalyst powders supported on carbon tape.

High-resolution transmission electron microscopy (HR-TEM) experiments were carried out to study the fine morphology of the Pd nanoparticles dispersed in catalysts, using a FEI TECNAIG² Microscope operated at 200 kV.

The specific surface area and the mean pore diameter of the catalysts were determined by nitrogen adsorption in accordance with the BET method, with a Micromeritics ASAP 2010 instrument. The BET surface area determinations were based on six measurements at relative pressures of N₂ in the range of 0.05~1.00.

2.4 Measurements of catalytic performance

Catalytic activity tests were performed in a continuous-flow fixed-bed microreactor. A glass tube with an inner diameter of 6 mm was chosen as the reactor tube. About 300 mg catalyst with the average diameter of 20~40 mesh was placed into the tube. The reaction gas mixture consisting of 1 vol.% CO balanced with air was passed through the catalyst bed at a total flow rate of 50mlmin⁻¹. A typical weight hourly space velocity (WHSV) was 10000 mlg⁻¹h⁻¹. The composition of the influent and effluent gas was detected with an online GC-7890II gas chromatograph equipped with a thermal conductivity detector. As we all know, CO oxidation reaction is accompanied by a reduction in the number of moles. In this paper, this change of moles was neglected. Therefore, the CO conversion was calculated based on the outlet CO:

$$\text{Conversion of CO\%} = \frac{([\text{CO}]_{\text{in}} - [\text{CO}]_{\text{out}})}{[\text{CO}]_{\text{in}}} \times 100\%$$

3 Results and discussion

3.1 Characterization of CSs

3.1.1 SEM analysis

Fig.1 shows SEM images and size histograms of CSs which are prepared by different concentrations of glucose solution. When concentration of glucose precursor was 0.1 molL^{-1} , regular spherical shapes could be formed with $0.42\mu\text{m}$ average diameter, but carbon spheres was aggregated and outer surfaces of CSs was uneven. With increasing of glucose concentration, the size of CSs increased and the surface of carbon spheres became very smooth without cracks, but many aggregated carbon spheres could be found from Fig.1b. The carbon sphere with uniform size and smooth outer surface were obtained until concentration of glucose precursor was 1.0 molL^{-1} , the average diameter of carbon sphere was $1.52\mu\text{m}$. As the glucose concentration further increased, the size of CSs increased and the average diameter of CSs was $4.95 \mu\text{m}$, but the particle size of CSs was not homogeneous (from Fig.1d).

3.1.2 BET

The N_2 adsorption-desorption isotherms of carbon spheres with different size is shown in Fig.2. According to the IUPAC classification, the isotherms of CSs from Fig.2 were type III. The adsorbed amount was almost zero at relatively low pressures. This suggested the existence of a few micropores. A hysteresis loop at relatively high pressures ($P/P_0 > 0.9$) emerged because of the appearance of macropores ($>50 \text{ nm}$). However, based on the SEM images, CSs had a non-porous surface. Therefore, this

might be caused primarily by the slits on the CSs [15, 20]. The textural properties of CSs which are prepared by different glucose concentrations are summarized in Table 1. From the Table 1, the BET surface areas of CSs which were prepared by 0.1 molL⁻¹, 0.5 molL⁻¹, 1.0 molL⁻¹ and 1.5 molL⁻¹ glucose solutions were 4.70 m²g⁻¹, 3.11 m²g⁻¹, 6.00 m²g⁻¹ and 4.65 m²g⁻¹, respectively. As we all know, the BET surface areas of CSs decrease with increasing of glucose concentration. But carbon spheres prepared by 0.1 molL⁻¹ and 0.5 molL⁻¹ glucose concentration were a bit aggregated, which was the main reason for BET surface areas decreased of CSs.

3.1.3 TEM and SEM analysis

TEM image of CSs, SEM and TEM images of Pd-Fe/CSs catalyst (CSs prepared by 1.0 molL⁻¹ glucose solutions) are investigated and the result is shown in Fig.3. From Fig.3a, it was observed that the synthesized carbon sphere was a solid sphere. Outer surface was smooth, which also indicated the result of Fig.2 was caused by the slits on the CSs. However, it was clearly seen from Fig.3b that the majority of the CSs surface was covered by Pd-Fe composites, and the size of Pd-Fe composites was 10-20 nm. This result was testified in SEM of Pd-Fe/CSs catalyst (see Fig.3d). Additionally, in order to directly investigate the Pd distribution in the sample, the TEM-EDS mapping image is revealed in Fig.3c. It can be seen that Pd atoms are distributed uniformly over the entire observed area of the sample.

3.2 The effect of carbon spheres size on the activity of CO oxidation

Fig.4 shows the results of CO oxidation over Pd-Fe/CSs catalysts with different particle sizes. From Fig.4, the higher reaction temperature was, the better the catalytic

activities was. The total conversion temperature (T_{100}) was 75 °C, 85 °C, 45 °C, 50 °C and 65 °C corresponding to the catalysts of Pd-Fe/CSs (0.42 μm), Pd-Fe/CSs (0.63 μm), Pd-Fe/CSs (1.52 μm), Pd-Fe/CSs (4.95 μm) and Pd-FeOx, respectively. It was obvious that the addition of CSs could improve activity for CO oxidation when the particle sizes of CSs were 0.42 μm , 1.52 μm and 4.95 μm . As we all know, larger surface area of support not only is conducive to load and disperse of Pd-Fe nanoparticles, but also favorable for the adsorption and diffusion of reactants and products. All of these are helpful for CO oxidation. Compared with Fig.2, Table 1 and Fig.4, it was easy to find that the activity improved along with the increase of surface area of support. This meant that the activity was direct factor to surface area of support. But sample a and sample d, having almost the same surface areas, exhibited very different T_{100} values. It evidenced the surface area was not the only factor. The surface chemical species, surface active oxygen and the distribution of active components may lead to great difference of catalyst activity.

3.3 The effect of calcination temperature on the activity of CO oxidation

Fig.5 shows the reaction results of CO oxidation over various Pd-Fe/CSs catalysts which are calcined at different temperature. Obviously, Pd-Fe/CSs catalysts exhibited high activity for CO oxidation and that the reaction activity increased gradually with the increase of calcination temperatures at first, and then decreased. It was observed T_{100} were 45 °C, 40 °C, 35 °C and 70 °C for catalysts which were calcined at 60 °C, 150 °C, 200 °C and 300 °C, respectively. In order to further study the effect of calcination temperature on CO oxidation, all catalysts are characterized by

XRD and XPS.

Fig.6 shows the XRD patterns of a series of catalysts which are prepared at different calcination temperatures. As we all know, the palladium species was the active composition in Pd catalyst. However, no characteristic diffraction peaks of Pd particles appeared in all catalysts, this showed that Pd species were dispersed highly. Diffraction peaks at $2\theta = 18.5^\circ, 30.8^\circ, 35.2^\circ, 43.0^\circ, 57.5^\circ$ and 62.7° were assigned to iron hydroxide (JCPDS PDF#22-0346) and it could be observed for Fig.6a. In addition, with increasing of calcination temperatures the intensity of iron hydroxide peaks decreased, XRD peaks at 18.5° disappeared from Fig.6b. It was clearly noticed at Fig. 6c that the peaks of iron hydroxide disappeared completely, one broad peak at 35.7° assigned to (211) crystalline plane of FeO(OH) was observed (JCPDS PDF#18-0639) [21]. It meant that Fe(OH)₃ phases converted to FeO(OH). When the catalyst was heated to about 300 °C, two Fe₂O₃ species were observed from Fig.6d. The peaks at $30.2^\circ, 35.6^\circ, 43.2^\circ$ and 53.7° was assigned to maghemite-C (JCPDS PDF#39-1346), and other peaks at $24.1^\circ, 33.1^\circ, 35.6^\circ, 40.8^\circ, 49.4^\circ, 54.1^\circ, 57.6^\circ, 62.4^\circ$ and 64.0° was assigned to hematite (JCPDS PDF#33-0664). Calcined process of catalysts was the process of transformation from iron hydroxide to iron oxide. By comparing the result of Fig.5, it was observed that FeO(OH) species were helpful for the increase of activity.

To demonstrate active phases of the catalysts which involved CO oxidation and variation of the surface species during catalytic reaction in detail, XPS was used to investigate chemical states of surface atoms in catalysts as well as composition and

related distribution of the surface elements. The Pd-Fe/CSs catalysts calcined at different temperature are tested by XPS, and the results are shown in Table 2 and Fig.7.

Fig.7A shows the XPS spectra of Pd 3d for the Pd-Fe/CSs catalysts calcined at different temperature. It was obvious that the peaks of Pd 3d shifted to the high binding energy with increases of calcination temperature. The Pd 3d spectrum shown in Fig. 1Aa was composed of one spin-orbit split doublet, which was assigned to bivalent Pd (PdO) [22]. With increases of calcination temperature, tetravalent Pd (PdO₂) appeared in Pd-Fe/CSs catalysts. The calculated percentages of tetravalent Pd (PdO₂) are listed in Table 2. It was very clear to see that the percentage of tetravalent Pd (PdO₂) increased with increases of calcination temperature. By comparing the result of Fig.5, it was observed that PdO₂ is the main species on Pd-Fe/CSs catalysts.

Fig.7B shows the XPS spectra of Fe2p for the Pd-Fe/CSs catalysts calcined at different temperature. Whether the catalysts were calcined, only one binding energy of Fe2p appeared in the XPS spectra. But the catalysts calcined at different temperature had different binding energies. All four catalysts had binding energies at 710.76 eV, 710.78 eV, 710.86 eV and 711.23eV, corresponding to calcination temperature at 60 °C, 150 °C, 200 °C and 300 °C, respectively [23]. By comparing with the result of Fig.6, Fe species of the catalysts calcined at 60 °C, 150 °C, 200 °C and 300 °C were Fe(OH)₃, Fe(OH)₃, FeO(OH) and Fe₂O₃, respectively. As we all know, FeO(OH) could store more activity oxygen than Fe(OH)₃ and Fe₂O₃ [24]. So the catalyst calcined at 200 °C exhibited superior activity of CO oxidation.

Fig.7C shows the XPS spectra of O 1s for the Pd-Fe/CSs catalysts calcined at different temperature. In this case three peaks (O, O', O'') could be identified by the deconvolution of the O1s spectra. The binding energy at 529.85 eV (O) was assigned to O²⁻ in the catalysts lattice, whereas the binding energy at 531.44 eV (O') was assigned to surface adsorbed oxygen such as O⁻ or OH⁻ [25, 26]. The binding energy above 533.29 eV (O'') was associated with adsorbed molecular water [25, 26]. Usually, a higher oxygen adspecies concentration on the catalyst surface is beneficial for the enhancement in catalytic activity [27]. So the relative content of the surface adsorbed oxygen species in the total surface oxygen can be estimated from the relative area of the sub-peak. The results are shown in Table 3. It was obvious that the relative content of the adsorbed oxygen species on Pd-Fe/CSs catalyst calcined at 200 °C was highest. As suggested above, Pd-Fe/CSs catalyst calcined at 200 °C had superior activity of CO oxidation.

3.4 The effect of Pd loading on the activity of CO oxidation

The effects of Pd loadings on the catalytic activity of Pd-Fe/CSs catalysts for the CO oxidation are investigated, and the results are shown in Fig.8. When Pd loading was below 0.7%, the CO conversion was affected obviously by the Pd loading. This indicated PdO₂ nanoparticles were the active composition in Pd-Fe/CSs catalysts. When Pd loading further increased the CO conversions over Pd-Fe/CSs catalyst had a modest increase. This was because that the palladium nanoparticles agglomerated easily if loading content of precious metal was too high, which was not helpful for increase of catalyst activity.

3.5 The effect of H₂ reduction on the activity of CO oxidation

In order to investigate the influence of pre-reduction on catalytic performance, the Pd-Fe/CSs catalyst (the optimal catalyst according to above research) are further reduced at 50°C in the stream of hydrogen gas with a rate of 30 mLmin⁻¹ for 1h, and then are cooled in hydrogen atmosphere to room temperature. It was shown that the performance of the reduced catalyst (Pd-Fe/CSs-R catalyst) was lower compared with the unreduced Pd-Fe/CSs catalyst (Fig.9). This could be explained by the XPS results.

The XPS spectra of Pd-Fe/CSs and Pd-Fe/CSs-R are presented in Fig.10 and Table 3. Fig.10A shows the XPS spectra of Pd3d for Pd-Fe/CSs and Pd-Fe/CSs-R catalysts. The Pd3d spectrum shown in Fig.10Aa was composed of two doublets, (u₀, u₂), (u₁, u₃) corresponding to the emission from the spin-orbit split 3d_{3/2} and 3d_{5/2} core levels. The two doublets (u₀, u₂), (u₁, u₃) were assigned to bivalent Pd (PdO) and tetravalent Pd (PdO₂), respectively. After H₂ reduction, three doublets, (v₀, v₃), (v₁, v₄), (v₂, v₅) were observed from Fig.10Ab, which was assigned to zerovalent (Pd⁰), bivalent Pd (PdO) and tetravalent Pd (PdO₂), respectively [21]. According to results of Fig.5 and Fig.7, PdO₂ is the main species on Pd-Fe/CSs catalysts. The calculated percentages of PdO₂ are listed in Table 2. It could be seen that the portions of PdO₂ component and the surface loading of Pd in the Pd-Fe/CSs catalyst was relatively high.

The spectra shown in Fig.10B revealed the characteristic spin-orbit splitting of Fe (2p) core levels [Fe (2p_{3/2}) and Fe (2p_{1/2})]. Here attention was only concentrated to the Fe (2p_{3/2}) core level electrons because it gave the spatial arrangement of the iron

species. From Fig.10Ba, only one peaks appeared at around 710.81 eV, which was assigned to characteristic peaks of FeO(OH) [22]. After H₂ reduction, the XPS peaks site Fe species had been no altered. As XPS was a surface sensitive technique so it gave an idea about the surface enrichment of FeO(OH) site. This surface enrichment of FeO(OH) was advanced oxidation sites on catalyst surface. The percentages of FeO(OH) are listed in Table 2. It could be seen that the FeO(OH) surface component in the Pd-Fe/CSs catalyst was relatively high.

Fig.10C shows the O (1s) core level XPS spectra of Pd-Fe/CSs and Pd-Fe/CSs-R catalysts. As suggested above, The peak O at 529.85 eV (BE), O' at 531.44 eV (BE) O'' at 533.29 eV (BE) were assigned to O²⁻ in the catalysts lattice, surface adsorbed oxygen such as O⁻ or OH⁻ and adsorbed molecular water, respectively [25, 26]. The relative content of the surface adsorbed oxygen species in the total surface oxygen can be estimated from the relative area of the sub-peak, and the results are shown in Table 3. It could be noticed that the relative content of the adsorbed oxygen species on Pd-Fe/CSs catalyst was higher than that on Pd-Fe/CSs-R catalyst.

The researched results showed that Pd species were the key factors influencing the catalytic performance of Pd-Fe/CSs catalysts and surface area, surface adsorbed oxygen concentration, reducibility were direct factor to affect the catalytic performance of Pd-Fe/CSs. From Fig.1, Fig.2, Fig.3, Fig.4 and Table 1, CSs which were prepared by 1.0molL⁻¹ glucose solution had highest BET surface area. When CSs were used as support, the catalyst had superior activity of CO oxidation. This was because high surface area of support was helpful for loading of Pd-Fe species.

According to the result of activity and characterization, it could be found that PdO₂ was the main species on Pd-Fe/CSs catalysts, amorphous FeO(OH) was more helpful for CO oxidation than crystal Fe(OH)₃ and Fe₂O₃. A higher oxygen adsorbed species concentration on the catalyst surface was beneficial for the enhancement in catalytic activity. There was a relatively high pressure of O₂ in this paper. According to related literatures [28], the FeO(OH) makes large amounts of weakly adsorbed oxygen available at the support surface. This oxygen is then able to compete with the lattice oxygen. At low CO pressures, competition of lattice oxygen on the Pd surface may occur. Therefore, for reaction mechanism of CO oxidation, maybe adhered to the Langmuir-Hinshelwood + Redox (see Fig.11): (a) CO firstly was adsorbed onto the tetravalent Pd; (b) the adsorbed CO on Pd species were more easily oxidized to CO₂ by catching the lattice oxygen (route 1 and 2) or adsorbed oxygen (route 3), meanwhile the catalysts produced the oxygen vacancy; (c) The oxygen vacancy would be replenished by O₂ of reaction gas to form the new active oxygen species and complete the redox cycle. FeO(OH) is main oxygen storage site in catalysts, so the route 1 is main route.

4 Conclusions

Catalytic properties of Pd-Fe catalysts supported on carbon spheres (CSs) were prepared and investigated for CO oxidation. The carbon spheres with controllable size were synthesized by hydrothermal method. The Pd-Fe/CSs catalysts were characterized by XRD, XPS, BET, SEM and TEM in detail. The experimental results revealed that particle size of carbon spheres, calcination temperature of catalysts, Pd

loadings and H₂ reduction had an effect on the activity of CO oxidation. By comparing activity results of catalysts with the result of characterization, the conclusions was as follows: (a) the bigger surface area of CSs was, the higher activity of the catalysts was; (b) PdO₂ was the main active species on Pd-Fe/CSs catalysts; (c) amorphous FeO(OH) was more helpful for CO oxidation than crystal Fe(OH)₃ and Fe₂O₃; (d) a higher oxygen adsorption concentration on the catalyst surface was beneficial for the enhancement in catalytic activity. At 1.0wt.% Pd loading, the Pd-Fe/CSs catalyst which was calcined at 200 °C without H₂ reduction had the highest activity.

Acknowledgements

The financial support of The National Basic Research Program of China (2013CB933201), West Light Foundation of The Chinese Academy of Sciences, Engineering Laboratory of Gansu Development and Reform Commission and Opening Project of State Key Laboratory for Oxo Synthesis and Selective Oxidation is gratefully acknowledged.

References

- [1] L.C. Wang, Q. Liu, X.S. Huang, Y.M. Liu, Y. Cao, K.N. Fan. *Appl. Catal. B: Environ.*, 88 (2009) 204-212.
- [2] M.S. Chen, Y. Cai, Z. Yan, K.K. Gath, S. Axnanda, D.W. Goodman, *Surf. Sci.*, 601(2007) 5326-5331.

- [3] S.M. McClure, D.W. Goodman, *Chem. Phys. Lett.*, 469 (2009) 1-13.
- [4] Y.Z. Li, Y. Yu, J.G. Wang, J. Song, Q. Li, M.D. Dong, C.J. Liu, *Appl. Catal. B: Environ.*, 125 (2012) 189-196.
- [5] A. Satsuma, K. Osaki, M. Yanagihara, J. Ohyama, K. Shimizu, *Appl. Catal. B: Environ.*, 132-133 (2013) 511-518.
- [6] A. Tomita, K. Shimizu, K. Kato, Y. Tai, *Catal. Commun.*, 17 (2012) 194-199.
- [7] W.L. Han, P. Zhang, Z.C. Tang, G.X. Lu, *Process Saf. Environ.*, in press, 2013.
- [8] H. Deng, X.L. Li, Q. Peng, X. Wang, J.P. Chen, Y.D. Li, *Angew. Chem. Int. Ed.*, 44 (2005) 2782-2785.
- [9] A.A. Deshmukh, S.D. Mhlanga, N.J. Coville, *Mater. Sci. Eng. R*, 70 (2010) 1-28.
- [10] H.K. Yu, G.R. Yi, J.H. Kang, Y.S. Cho, V.N. Manoharan, D.J. Pine, S.M. Yang, *Chem. Mater.*, 20 (2008) 2704-2710.
- [11] Z. Mehraban, F. Farzaneh, V. Dadmehr, *Mater. Lett.*, 63 (2009) 1653-1655.
- [12] C.M. Lei, W.L. Yuan, H.C. Huang, S.W. Ho, C.J. Su, *Synthetic Met.*, 161(2011) 1590-1595.
- [13] Q Lin, M Zheng, T Qin, R Guo, P Tian, *J. Anal. Appl. Pyrol.*, 89 (2010) 112-116.
- [14] Q. Wang, F. Cao, Q. Chen, C. Chen, *Mater. Lett.*, 59 (2005) 3738-3741.
- [15] M. Li, W. Li, S. Liu, *Carbohydr. Res.*, 346 (2011) 999-1004.
- [16] X. Wang, J. Liu, W. Xu, *Colloid. Surface A*, 415 (2012) 288-294.
- [17] S. Hinokuma¹, Y. Katsuhara, E. Ando, K. Ikeue, M. Machida, *Catal. Today*, 201 (2013) 92-97.
- [18] Y. Shen, G. Lu, Y. Guo, Y. Wang, Y. Guo, L. Wang, X. Zhen, *Catal. Commun.*, 18

(2012) 26-31.

[19] L.Q. Liu, B.T. Qiao, Y.D. He, F. Zhou, B.Q. Yang, Y.Q. Deng, *J. Catal.*, 294

(2012) 29-36.

[20] X.M. Sun, Y.D. Li, *Angew. Chem. Int. Ed.*, 43 (2004) 3827-3831.

[21] W. Han, P. Zhang, X. Pan, Z. Tang, G. Lu, *J. Environ. Chem. Eng.*, 1 (2013)

189-193.

[22] K. S. Kim, A. F. Gossmann, N. Winograd., *Anal. Chem.*, 46(1974) 197-200.

[23] C.D. wagner, W.M. Riggs, L.E. Davis, J.F. Moulder, G.E. Muilenberg, *Handbook of X-Ray Photoelectron Spectroscopy*, Physical Electronics Inc, USA, 1995.

[24] W. Han, P. Zhang, X. Pan, Z. Tang, G. Lu, *J. Hazard. Mater.*, 263 (2013) 299-306.

[25] Z.M. Liu, J.M. Hao, L.X. Fu, T.L. Zhu, *Appl. Catal. B: Environ.*, 44 (2003) 355-370.

[26] Z. Qu, F. Yu, X. Zhang, Y. Wang, J. Gao, *Chem. Eng. J.*, 229 (2013) 522-532.

[27] R.J.H. Voorhoeve, J.P. Remeika, D.W. Johnson, *Science*, 180 (1973) 62-64.

[28] E. Bekyarova, P. Fornasiero, J. Kašpar, M. Graziani, *Catal. Today*, 45 (1998) 179-183.

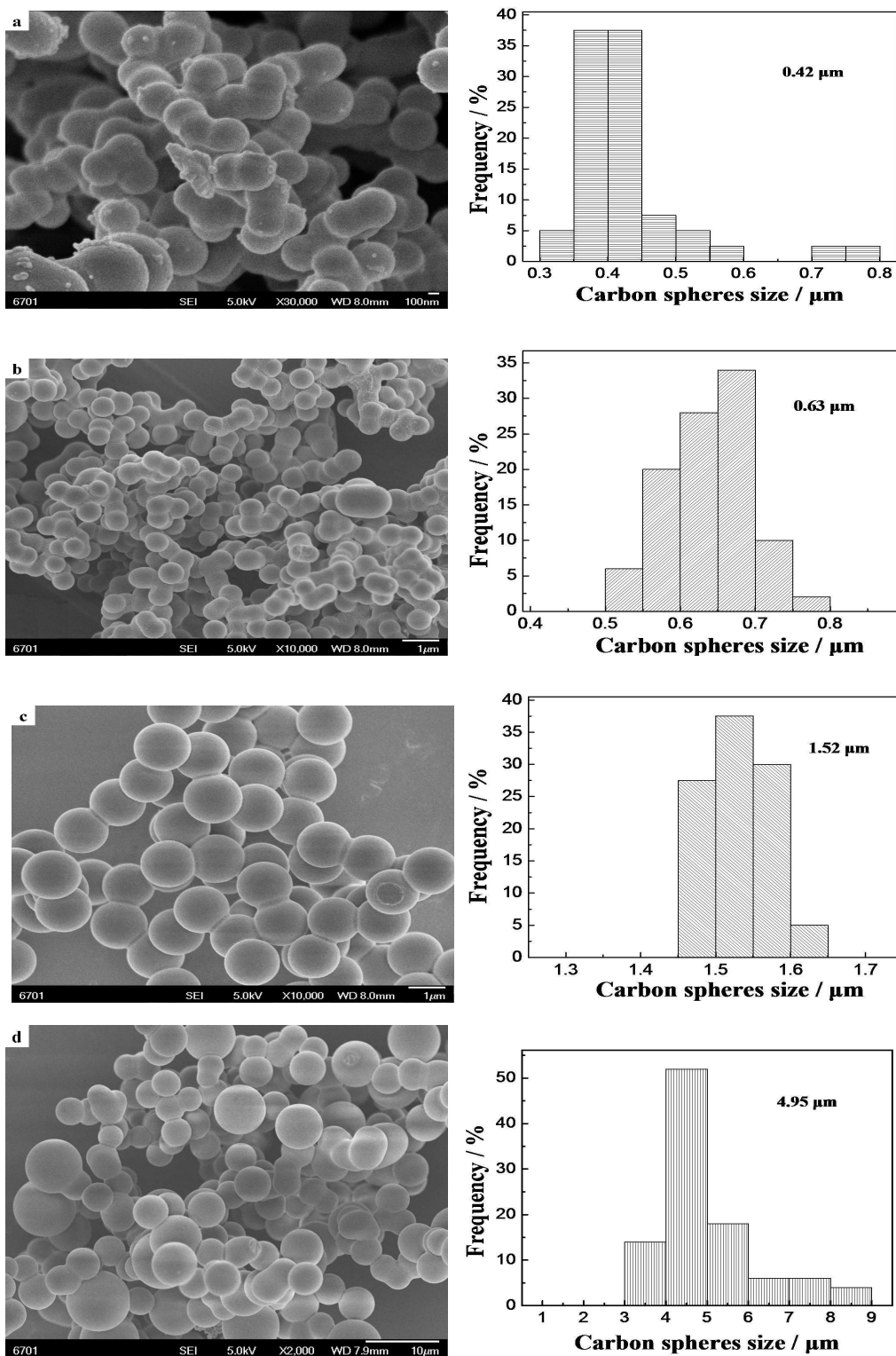


Fig.1 SEM images and particle size distribution of carbon spheres prepared by different glucose concentrations. (a) 0.1 molL⁻¹; (b) 0.5 molL⁻¹; (c) 1.0 molL⁻¹; (d) 1.5 molL⁻¹.

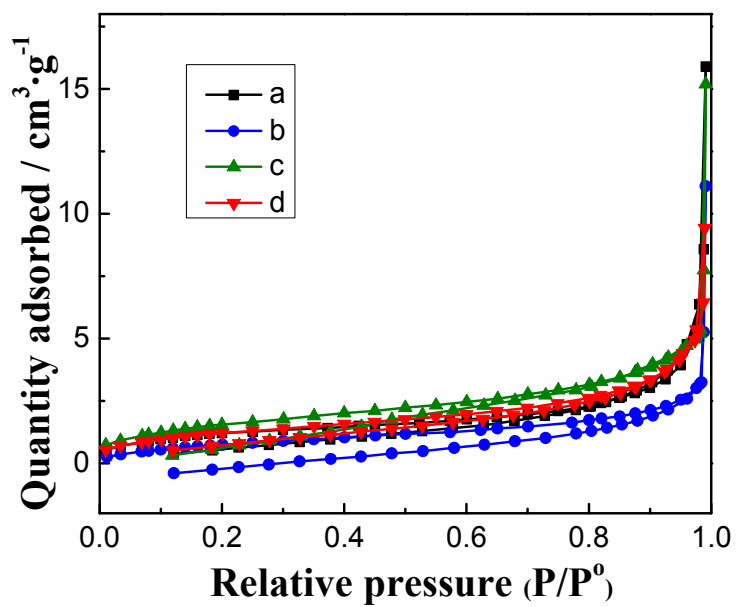


Fig.2 N₂ adsorption-desorption isotherms of carbon spheres prepared by different glucose concentrations. (a) 0.1 molL⁻¹; (b) 0.5 molL⁻¹; (c) 1.0 molL⁻¹; (d) 1.5 molL⁻¹.

Table 1 Pore structure parameters of carbon spheres prepared by different glucose concentrations

Sample	Glucose concentration (molL ⁻¹)	Surface area (m ² g ⁻¹)	Pore volume (cm ³ g ⁻¹)	Average pore diameter (nm)
a	0.1	4.70	0.00781	6.65
b	0.5	3.11	0.00466	5.99
c	1.0	6.00	0.00769	5.13
d	1.5	4.65	0.00760	6.54

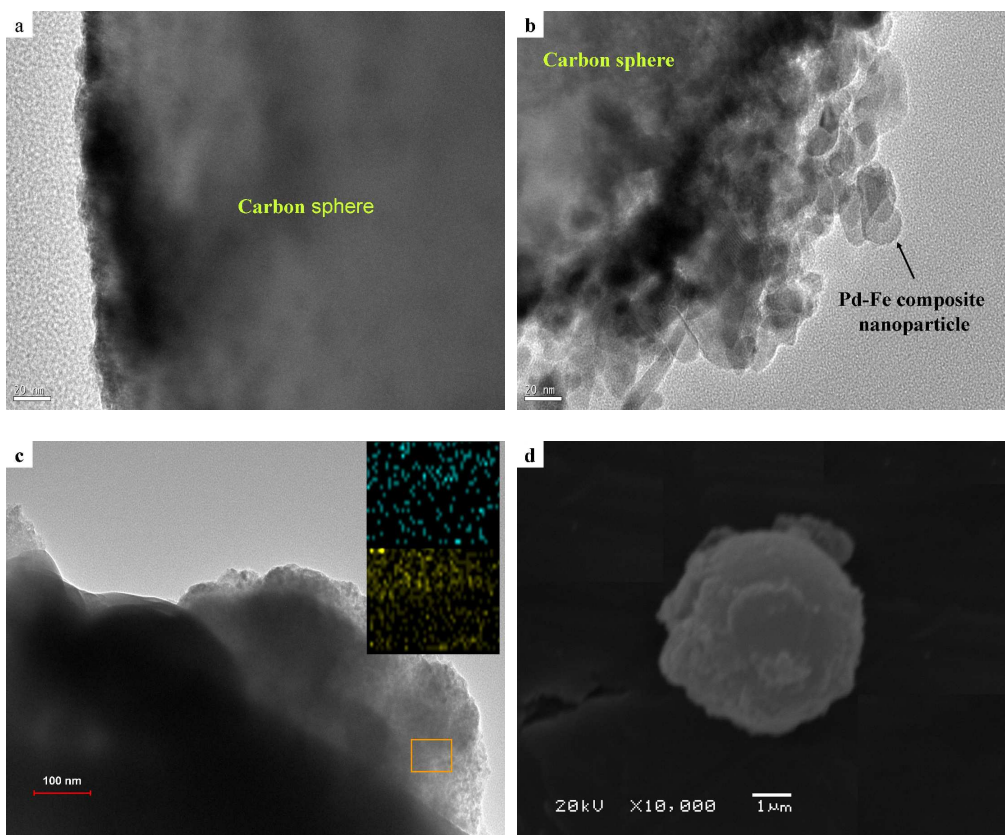


Fig.3 TEM image of carbon sphere (a) and Pd-Fe/CSs catalyst (b), TEM-EDS mapping image taken from a square region (blue stands for Pd while yellow stands for Fe) of Pd-Fe/CSs catalyst (c), SEM image of Pd-Fe/CSs catalyst (d).

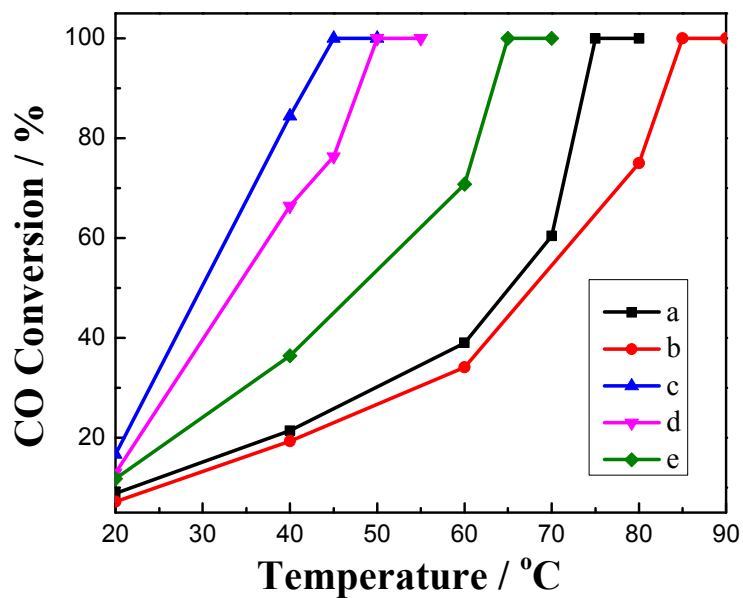


Fig.4 The effect of carbon spheres particle size on the activity of CO oxidation. (a) Pd-Fe/CSs (0.42 μm); (b) Pd-Fe/CSs (0.63 μm); (c) Pd-Fe/CSs (1.52 μm); (d) Pd-Fe/CSs (4.95 μm); (e) Pd-FeOx.

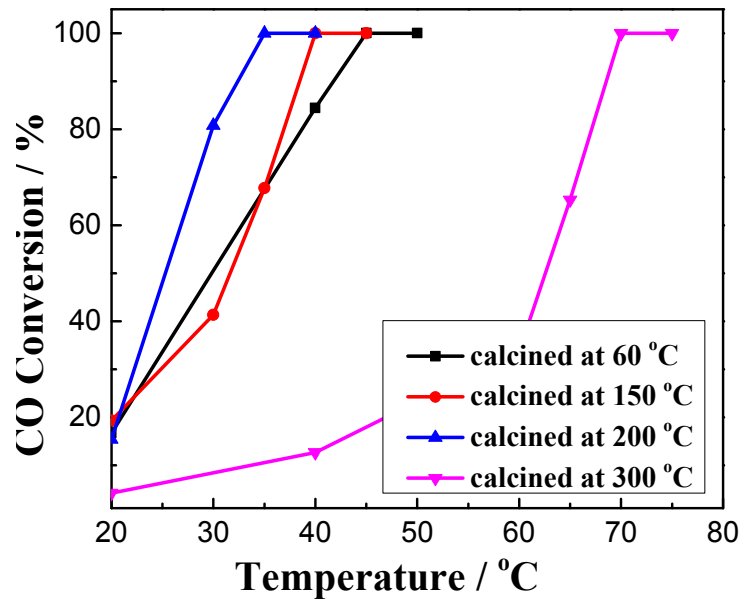


Fig.5 The effect of calcination temperature on the activity of CO oxidation.

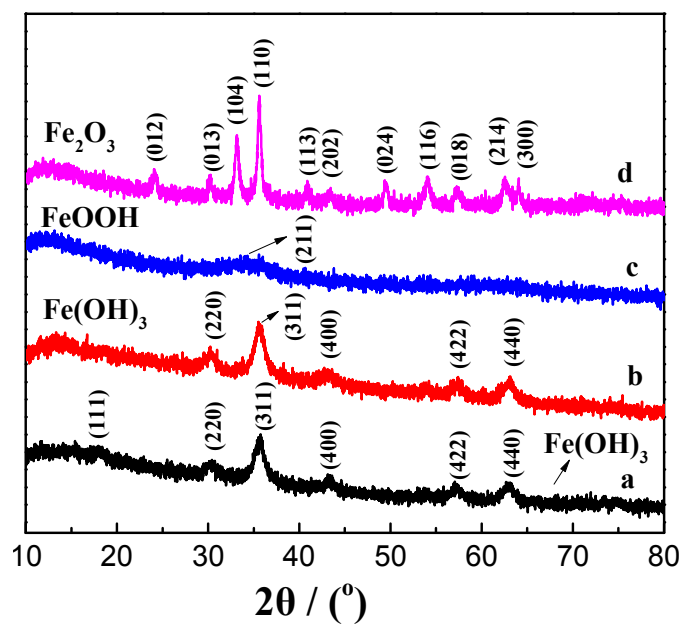


Fig.6 XRD patterns of Pd-Fe/CSs catalysts with different calcined temperatures.

(a) 60 °C; (b) 150 °C; (c) 200 °C; (d) 300 °C.

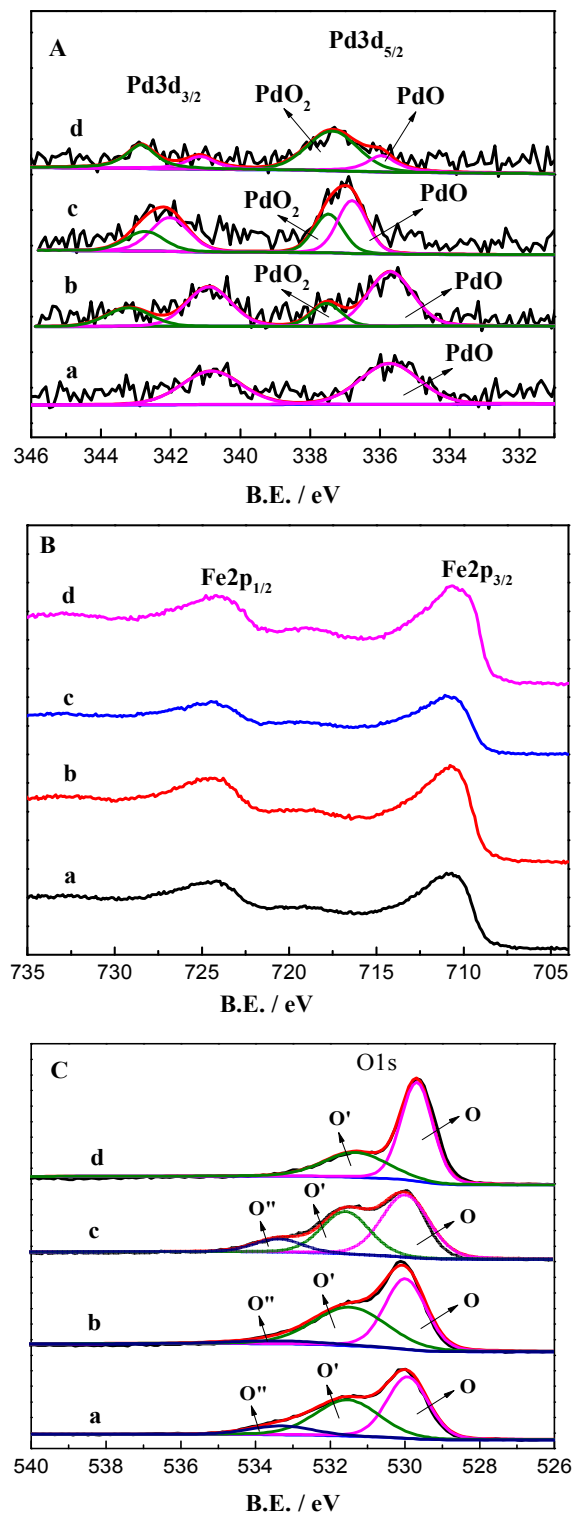


Fig.7 XPS spectra of Pd-Fe/CSs catalysts calcined at the different temperatures.

(a) 60 °C; (b) 150 °C; (c) 200 °C; (d) 300 °C.

Table 2 Chemical properties of the Pd-Fe/CSs catalysts calcined at different temperatures

Sample	Calcined temperature (°C)	$O_{\text{ads}}/(O_{\text{ads}} + O_{\text{latt}})$ or $(O^{\cdot} + O^{\cdot\cdot})/(O + O^{\cdot} + O^{\cdot\cdot})$	$\text{Pd}^{4+}/(\text{Pd}^{4+} + \text{Pd}^{2+})$	Fe content (%)	Pd content (%)
a	60	0.472	0	9.83	0.11
b	150	0.516	0.218	9.98	0.12
c	200	0.530	0.423	10.81	0.13
d	300	0.336	0.762	13.28	0.12

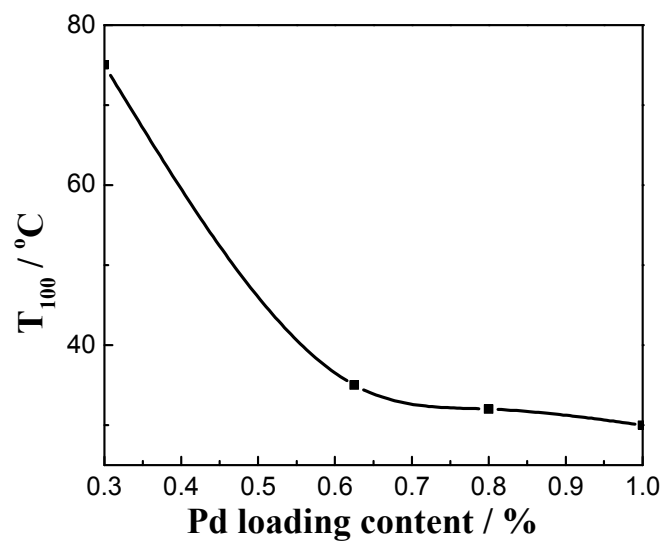


Fig.8 The effect of Pd loading amounts on the activity of CO oxidation

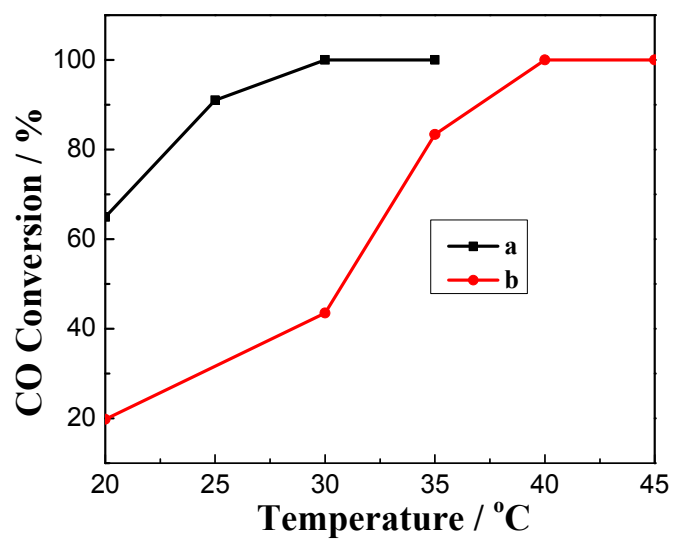


Fig.9 Catalytic activity of the catalysts before (a) and after (b) H₂ reduction for CO oxidation.

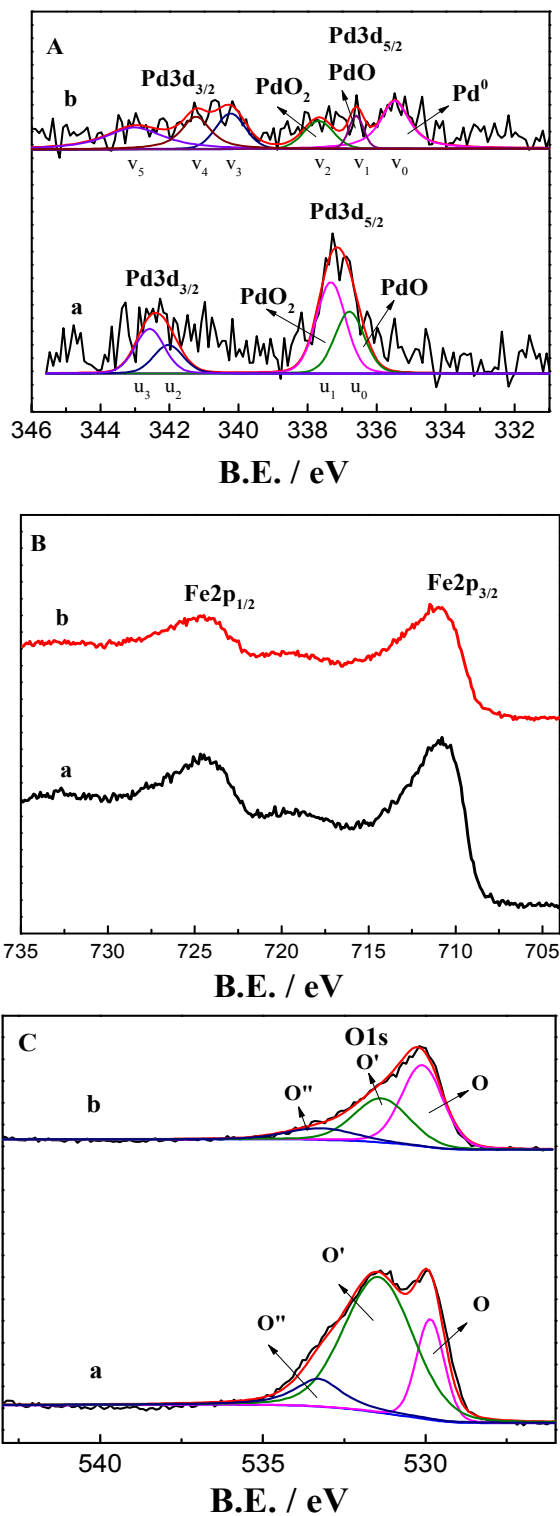


Fig.10 XPS spectra of the catalysts before (a) and after (b) H₂ reduction.

Table 3 Chemical properties of the catalysts

Sample	Catalyst	$O_{ads}/(O_{ads} + O_{latt})$ or $(O^{\cdot} + O^{\cdot\cdot})/(O + O^{\cdot} + O^{\cdot\cdot})$	Pd^{4+} $/(Pd^{4+} + Pd^{2+} + Pd^0)$	Fe content (%)	Pd content (%)
a	Pd-Fe/CSs	0.803	0.597	16.98	0.330
b	Pd-Fe/CSs-R	0.489	0.263	8.26	0.200

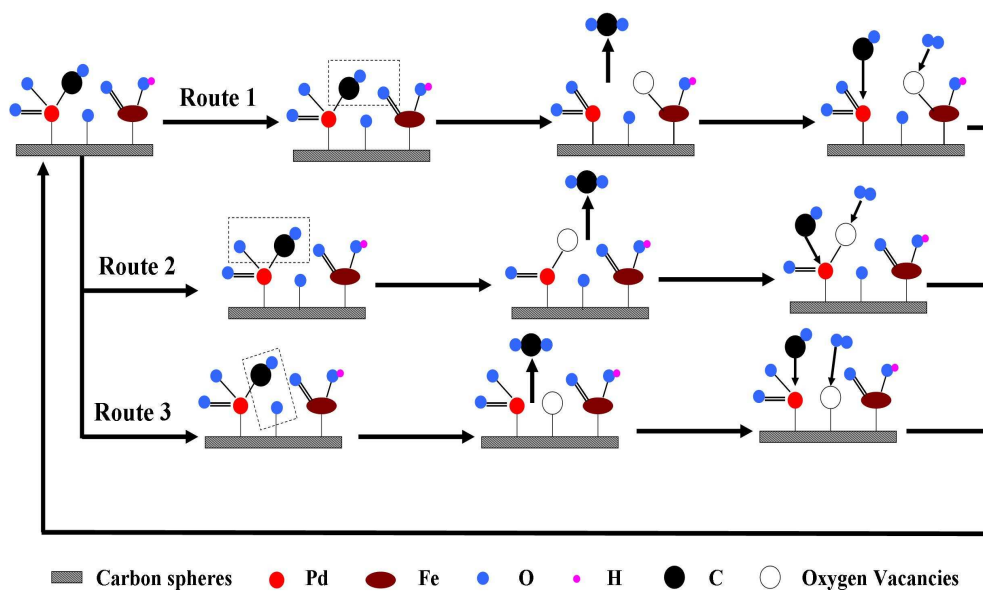


Fig.11 Reaction pathway illustration for CO oxidation over Pd-Fe/CSs.